ARL-TR-10382 ● JULY 2026

Segregation Modeling and Mitigation in Ultra-High-Strength Steels

by Heather Murdoch, Michael Rupinen, and Daniel Field

NOTICES

Disclaimers

The findings in this report are not to be construed as an official Department of the Army position unless so designated by other authorized documents.

Citation of manufacturer's or trade names does not constitute an official endorsement or approval of the use thereof.

Destroy this report when it is no longer needed. Do not return it to the originator.

ARL-TR-10382 ● JULY 2026

Segregation Modeling and Mitigation in Ultra-High-Strength Steels

Heather Murdoch, Michael Rupinen, and Daniel Field
DEVCOM Army Research Laboratory

REPORT DOCUMENTATION PAGE

1. REPORT DATE	2. REPORT TYPE	3. DATES COVERED	
		START DATE	END DATE
July 2026	Technical Report	Jan 2026	June 2026

4. TITLE AND SUBTITLE
Segregation Modeling and Mitigation in Ultra-High-Strength Steels

5a. CONTRACT NUMBER	5b. GRANT NUMBER	5c. PROGRAM ELEMENT NUMBER
5d. PROJECT NUMBER	**5e. TASK NUMBER**	**5f. WORK UNIT NUMBER**

6. AUTHOR(S)
Heather Murdoch, Michael Rupinen, and Daniel Field

7. PERFORMING ORGANIZATION NAME(S) AND ADDRESS(ES)	8. PERFORMING ORGANIZATION REPORT NUMBER
DEVCOM Army Research Laboratory ATTN: FCDD-RLA-MF Aberdeen Proving Ground, MD 21005	ARL-TR-10382

9. SPONSORING/MONITORING AGENCY NAME(S) AND ADDRESS(ES)	10. SPONSOR/MONITOR'S ACRONYM(S)	11. SPONSOR/MONITOR'S REPORT NUMBER(S)

12. DISTRIBUTION/AVAILABILITY STATEMENT
DISTRIBUTION STATEMENT A. Approved for public release: distribution unlimited.

13. SUPPLEMENTARY NOTES
ORCIDs: Heather Murdoch, 0000-0001-7710-0577; Michael Rupinen, 0009-0009-9438-9902; Daniel Field, 0000-0002-8890-4391

14. ABSTRACT
The composition of a segregated region as predicted from Scheil solidification modeling is used to determine potential effects of elemental segregation on both carbide and austenite stability in ultra-high-strength steels. This modeling approach captured both the increase in M_6C and fresh martensite, which were experimentally observed in segregation bands for a family of nickel–cobalt steels. Strong partitioning of molybdenum (Mo) and tungsten (W) promotes the formation of M_6C, and the austenite composition can also be enriched in both these and additional alloying elements, which impacts the austenite → martensite transformation. Modeling of the martensite start (M_S) temperature for the segregated compositions showed a depression of the M_S with increased Mo and W content in solution, which would lead to an incomplete transformation. However, the increased formation of M_6C with increasing alloy content actually reduced the effect on the M_S temperature as the enriched elements are drawn to the carbide instead of remaining in austenite, offering a possible tool to balance the competing segregation issues.

15. SUBJECT TERMS
interdendritic composition, Schiel–Gulliver solidification, nickel–cobalt steels, Ni-Co steels, ultra-high-strength steels, UHSS, martensite transformation, M_S, Sciences of Extreme Materials

16. SECURITY CLASSIFICATION OF:			17. LIMITATION OF ABSTRACT	18. NUMBER OF PAGES
a. REPORT	b. ABSTRACT	C. THIS PAGE		
UNCLASSIFIED	UNCLASSIFIED	UNCLASSIFIED	UU	33

19a. NAME OF RESPONSIBLE PERSON	19b. PHONE NUMBER *(Include area code)*
Heather Murdoch	(520) 691-6293

STANDARD FORM 298 (REV. 5/2020)
Prescribed by ANSI Std. Z39.18

Contents

List of Figures

List of Tables

1. Introduction

The microstructure of a steel component is inherited from the solidification structure of the alloy during the casting process. Compositional variations across the cast ingot can be severe, depending on cooling rates, the diffusion rates of the alloying elements involved, and the solidification order of phases. These compositional variations then lead to local variations in microstructure, which will impact the properties of the material. Appreciable macro- and micro-segregation can lead to low fracture and impact toughness, reduced corrosion resistance, heat treatment distortion, and inconsistent hardness and hardenability. Macro-segregation is segregation observed across the ingot, caused by convection in the multiphase mushy zone driven by compositional and temperature differences between liquid and solid and is not easily addressed short of remelting the material. Micro-segregation is typically across dendrites, e.g., differences between the dendrite core and interdendritic region.[1] An example is shown in Figure 1.

Figure 1. Light optical image of micro-segregation showing the dendritic cast structure in an ultra-high-strength steel (UHSS) alloy that was cast, forged, and then austenitized at 950 °C for 1 h and air-cooled.

As steel alloys become enriched in alloying elements, the potential for segregation increases. One way of expressing the relative tendency and severity of segregation is the segregation ratio—a measure of the composition of an alloying element in a segregated region relative to its average global composition. Some measured segregation ratios for solute elements in various steels are summarized in Figure 2.[1–15] Local enrichment of these elements promotes the formation of deleterious phases that will impact the toughness (i.e., the stabilization of austenite or increasing the propensity for carbide nucleation). For example, over double the

volume fraction of $M_{23}C_6$ carbides were found in the interdendritic region compared with the dendrite core in a low-alloy martensitic steel.[16] $M_{23}C_6$ and M_6C are deleterious to toughness in high-strength, high-toughness steels and $M_{23}C_6$ formation can also lead to sensitization or reduced corrosion resistance of certain alloys. Both carbides are face-centered cubic with very large lattice parameters (>7 Å), leading to poor registry of the carbide with the martensitic matrix (~2.8 Å). The $M_{23}C_6$ is enriched in chromium (Cr) and tungsten (W) while the M_6C is enriched in molybdenum (Mo) and W. Formation of M_6C and $M_{23}C_6$ in segregated regions also detracts from the formation of other precipitates such as M_2C carbides, which can provide an efficient strengthening effect.

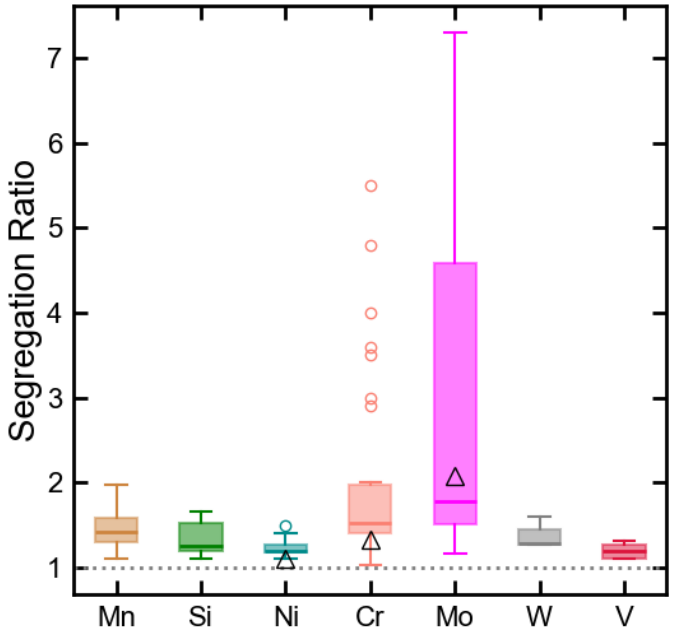

Figure 2. Summary of segregation ratios from literature[2–7]; measured segregation for AerMet100[4] is indicated by the triangle points. Note: The Cr outlier points are all in high-carbon (C) (>0.7 wt%) steels (e.g., white cast iron).

Mitigation strategies for segregation include additional processing steps: heat treatments, deformation processing (e.g., forging or rolling), and remelting. The effectiveness of normalization heat treatments depends on the mobility of the elements involved; unfeasible times and temperatures may be required to fully homogenize the microstructure. For example, heat treatment was sufficient to redistribute C, but not Cr and Mo, in a low-alloy steel[13]; and homogenization treatments improved impact properties but there was still visible variation in microstructure in a pressure vessel steel.[10] Even if chemical homogeneity is achieved, a consequence of the extended heat treatment could be significant grain growth that will negatively affect properties (i.e., raising the ductile to brittle transition temperature). Deformation methods like upset forging of the cast ingot

will reduce the diffusional distance between segregated regions, making normalizing somewhat more effective. The most successful, but costliest, approach is vacuum arc remelting (VAR) in which the ingot is remelted in a vacuum and is effective at both practically eliminating centerline porosity and segregation.[17]

While thermomechanical work, homogenization treatments, and remelting may be used to mitigate segregation effects, many applications exist where one or all of these treatments are impractical due to cost and other practical constraints. Effective modeling approaches for segregation incorporated with alloy and process design can be used to both minimize segregation and assess the impact of unavoidable segregation (e.g., predict the difference between the microstructure from segregated and bulk compositions and its potential role in affecting a property of interest).

2. Experimental Alloys

In this work we explore the effects of alloying elements on segregation in a family of nickel–cobalt (Ni-Co) steels where Mo, Cr, and W are used to increase strength through formation of M_2C carbides. However, the desire to increase these elements for the M_2C strengthening conflicts with the need to avoid segregation, as they are all strong segregators (Figure 2), especially Mo. The compositions of selected alloys are shown in Table 1. The Generation (Gen) 3 alloy has the highest amount of Mo, Cr, and W and had extremely obvious segregation banding compared with the other alloys (Figure 3). The microstructure difference between the segregation band (dark-etching) and non-segregated (light-etching) regions of the material is highlighted in Figure 3. The non-segregated regions are tempered martensite with small carbides while the segregation band has regions of both fresh and tempered martensite and large hexagonal carbides (identified as M_6C). Enrichment of alloying elements in the segregated region stabilizes the M_6C carbides to temperatures well above the austenitization temperature while concurrently stabilizing the austenite to temperatures well below room temperature (leading to incomplete transformation during quenching). Some of the retained austenite is presumably destabilized during the multistep heat treatment, leading it to transform to fresh martensite during cooling from the tempering temperature. The combination of undissolved carbides, fresh martensite, and retained austenite can be problematic for maintaining high toughness as the segregated areas may be more prone to low-energy crack propagation modes. The effects of the segregated composition on both the carbides and the martensitic transformation will be explored for developmental alloys with various modeling techniques, with an illustration of how to implement them for design of alloys.

Table 1. Composition of designed and investigated alloys.

Alloy	C	Mn	Si	Cr	V	Mo	Ni	Co	W	Fe
AerMet100	0.22	0.01	0.01	3.0	. . .	1.19	11.22	13.38	. . .	70.97
Gen1 base	0.27	0.34	0.04	1.12	0.11	1.07	7.52	4.61	. . .	84.92
Gen1 W	0.29	0.34	0.03	1.15	0.11	1.09	7.29	4.60	0.47	84.63
Gen1 CrMo	0.31	0.34	0.03	1.76	0.11	1.74	7.45	4.41	. . .	83.85
Gen1 CrMoW	0.28	0.34	0.03	1.76	0.11	1.73	7.47	4.54	0.47	83.27
Gen2	0.3	0.33	0.08	2.75	0.11	1.48	7.45	4.62	. . .	82.91
Gen2 + W	0.28	0.3	0.08	2.75	0.11	1.4	7.77	4.95	1.07	81.21
Gen3	0.28	0.3	0.05	3.01	0.11	1.9	7.68	4.89	1.02	80.68

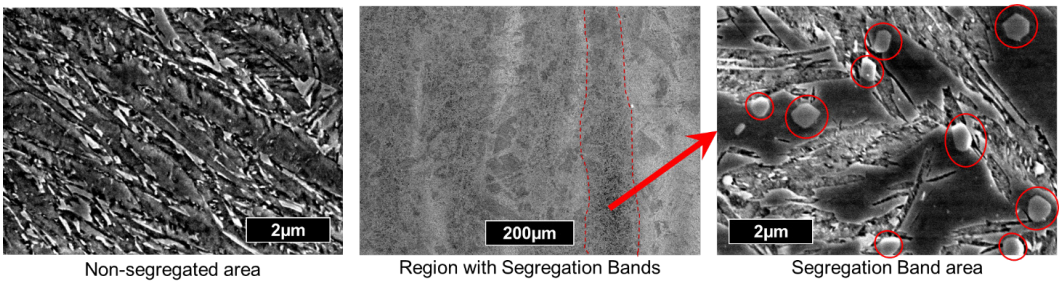

Figure 3. Example scanning electron microscope (SEM) images (Nital etch) of segregation bands from the Gen3 alloy following austenitization (1000 °C) and tempering. The center image is a large-area SEM image of segregation banding; dark areas are more highly segregated regions. Within the segregation band, red circles highlight the M_6C carbides; the flat dark regions are fresh martensite.

3. Methods

Thermo-Calc 2025a software[18] was used to model the solidification path using the TCFE10 and MOBFE5 databases and the Scheil module. The Diffusion Controlled Transformations (DICTRA) module was also briefly used for a comparative study. The composition of the liquid changes as the material solidifies, with elements partitioning from liquid to austenite. There are several different simulation types for Scheil simulations, summarized in Table 2. For classic Scheil, diffusion in the liquid phase is assumed to be infinitely fast, and diffusion in the solid phase is zero. Some elements can be selectively described as "fast diffusers" where diffusion in both the solid and liquid is infinitely fast; this is typically reserved for interstitial elements like C and nitrogen (N). Back diffusion allows for diffusion in the solid phases and requires a mobility database for the substitutional elements, as well as a user input value for the ingot cooling rate and dendrite spacing.

Table 2. Diffusion for the different Scheil simulation types.

Scheil type	Phase	Interstitial	Substitutional
		C	Co, Cr, Mo, Ni, W, Mn, Si, V
Classic	Liquid	∞	∞
	Solid	0	0
Classic + Fast diffuser	Liquid	∞	∞
	Solid	∞	0
Back diffusion	Liquid	∞	∞
	Solid	*Calc.*	*Calc.*
Back diffusion + Fast diffuser	Liquid	∞	∞
	Solid	∞	*Calc.*

An early work on segregation and homogenization in AerMet100[4] compared modeling approaches to predict the measured segregation across secondary dendrites and the time required for homogenization. The measured segregation for AerMet100 is indicated by the triangle points in Figure 2. The Classic Scheil method was qualitatively correct but strongly overestimated the segregation quantitatively. Further, a much larger solidification range (of 362 °C) was predicted than what was expected, which enabled the formation of carbides during solidification in the modeling results and is not supported by the experimental observations. The DICTRA module was also compared with Classic Scheil in Lippard et al.,[4] and simulations were mostly quantitatively correct but took approximately 20 times longer to calculate (and also required a reasonable estimation of dendrite spacing and cooling rate to align with results).

At the time of the work on AerMet100 by Lippard et al.,[4] the other types of diffusion were not yet integrated into the Scheil module. Now that they are, we consider the comparison of a more advanced Scheil prediction to DICTRA. The back diffusion calculation for Scheil also requires an estimate of dendrite spacing and cooling rate but is far less sensitive to the values; see the Appendix (Figures A-1 and A-2). Using the same parameters Lippard et al.[4] used for their DICTRA simulations—100-µm dendrite spacing and 0.5 °C/s cooling rate—we ran the Scheil with back diffusion and C as a fast diffuser; this predicts a much more reasonable solidification range of only 90 °C, and no carbide formation (Figure 4).

The changing volume fraction of liquid as a function of temperature is shown on the left-hand side of Figure 4. On the right-hand side of Figure 4, the composition of the liquid is shown, scaled by the bulk composition. As the fraction of liquid decreases, elements become increasingly segregated. Mo is the most strongly segregated, as expected. The elements Co and Ni are essentially the same (e.g., unsegregated, throughout solidification). The segregation ratios of the final fraction of liquid are still quantitatively higher than experimental measurements. However, even with the added diffusion calculations the Scheil simulation is orders of

magnitude faster than DICTRA. Running the current version of DICTRA with the same parameters as Lippard et al.[4] took approximately 200 min compared with approximately 3 min for Scheil. Further, the final segregated solidification state as predicted by DICTRA is no longer as close to the experimentally observed values (Table 3), as the thermodynamic and mobility databases have been significantly updated since the original work.

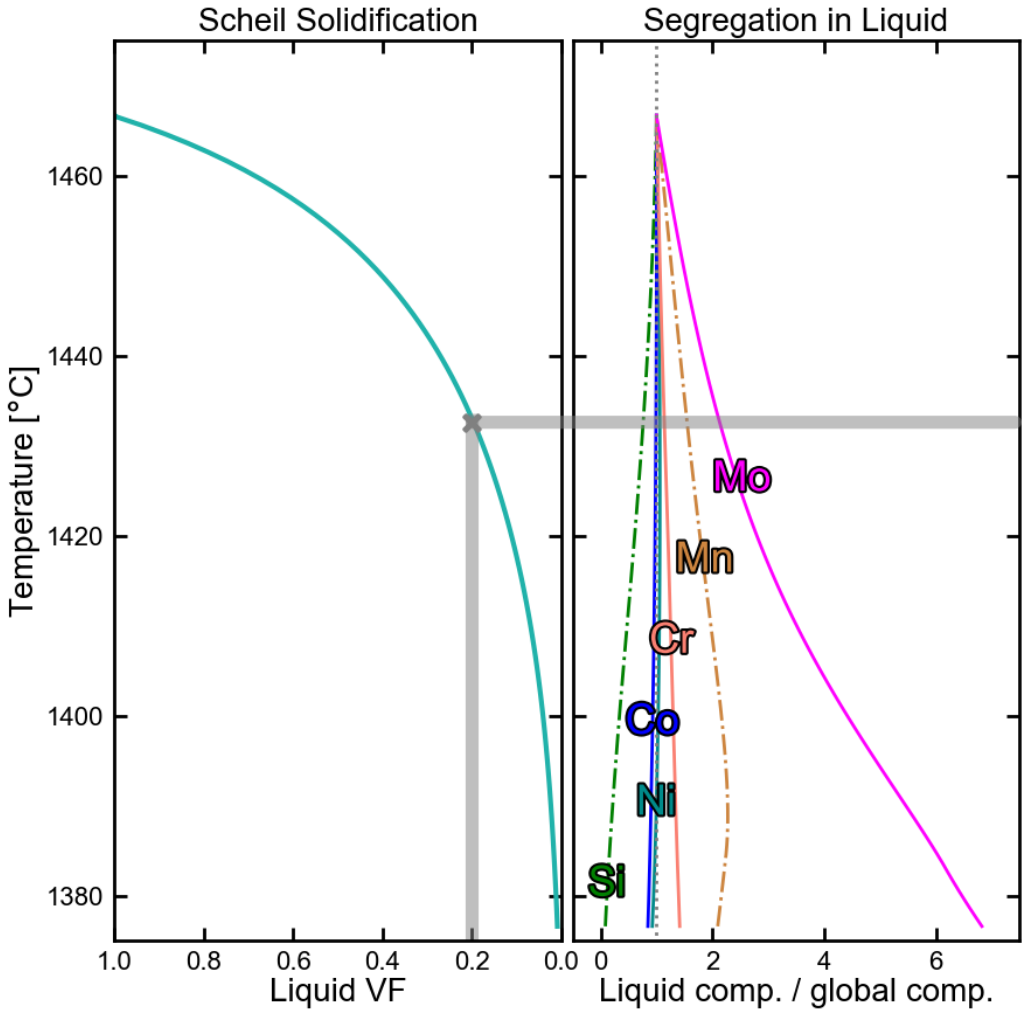

Figure 4. (Left) Scheil solidification curve for AerMet100, liquid only; (right) composition in liquid, scaled by global composition. Minor elements are dashed lines.

Several works[16,19–22] have proposed that a point in the solidification curve prior to completion should be used as the expected final segregated composition, as the physical and kinetic constraints of the interdendritic region will likely inhibit the continued solidification path at a certain point. Qualitatively, picking a composition at 15%–20% liquid remaining in the solidification path as the final "frozen" point has been successful in designing homogenization and austenitizing heat treatments to alleviate the impact of segregation. For example, Webb et al.[16] used the

composition profile from Scheil down to 20% liquid as input to a fluid dynamics model to predict homogenization behavior, which matched well with the experimental observations. And, in Field et al.[20,21] the toughness of a wrought ultra-high-strength martensitic CrNiMoV steel was improved by 75% using a heat treatment intended to dissolve the carbides expected from a segregation band of the composition represented by 15% liquid, rather than the global composition.

The segregation of the major elements in AerMet100 at 20% liquid (gray regions on Figure 4) is shown in Table 3 and compared with the experimental measurement.[4] There is good agreement supporting the argument that 15%–20% is a reasonable approximation of the segregated region.

Table 3. Segregation ratios of major elements in AerMet100.

Element	DICTRA ratio	20% DICTRA ratio	Scheil ratio	20% Scheil ratio	Exp. ratio
Mo	3.84	2.06	7.93	2.13	2.08
Cr	1.22	1.14	1.42	1.14	1.33
Ni	1.07	1.06	0.91	1.06	1.10
Co	1.01	1.01	0.84	0.99	1.00

Figure 4 and Table 3 show the substitutional alloying elements; C as an interstitial is not generally quantified due to experimental measurement challenges. Roy et al.[5] measured about a ratio of 1.5 for C segregation with electron probe micro-analysis. The Scheil and other predictive methods (e.g., Clyne–Kurz) likely overestimate C segregation. Models for considering segregation during solidification stop at the solidus temperature; however, the ingot continues to cool and is still at elevated temperatures for some time, which alloys for continued diffusion, particularly of a fast interstitial diffuser. Roy et al. showed that considering this continued temperature exposure could even out the C distribution, but not the substitutional elements. This is consistent with other reports where heat treatments were successful at redistributing C but not other elements.[13] Since any C segregation is likely able to be mitigated through reasonable temperatures and times through thermal processing treatments, we focus on the enrichment of the substitutional atoms and set the C content in the segregated region to be the same as the bulk. This approach was successful in modeling impacts of segregation in Athavale et al.[22]

The equilibrium phases predicted for the global composition of AerMet100 compared with the segregated (20% liquid) composition are shown in Figure 5; the temperature of the homogenization treatment used in the experimental work of Lippard et al.[4] is also indicated for reference. The bulk composition phases are solid lines, and the segregated phases are dashed lines. The M_6C carbide is predicted to

be stable in the segregated region, but not the global composition. This is due to the elevated Mo content in the segregated region (Table 3), as the carbide predominantly comprises Mo (Figure 6). The homogenization temperature chosen was well above the solvus temperatures of M_6C and $M_{23}C_6$ and no carbides were experimentally observed in Lippard et al.[4]

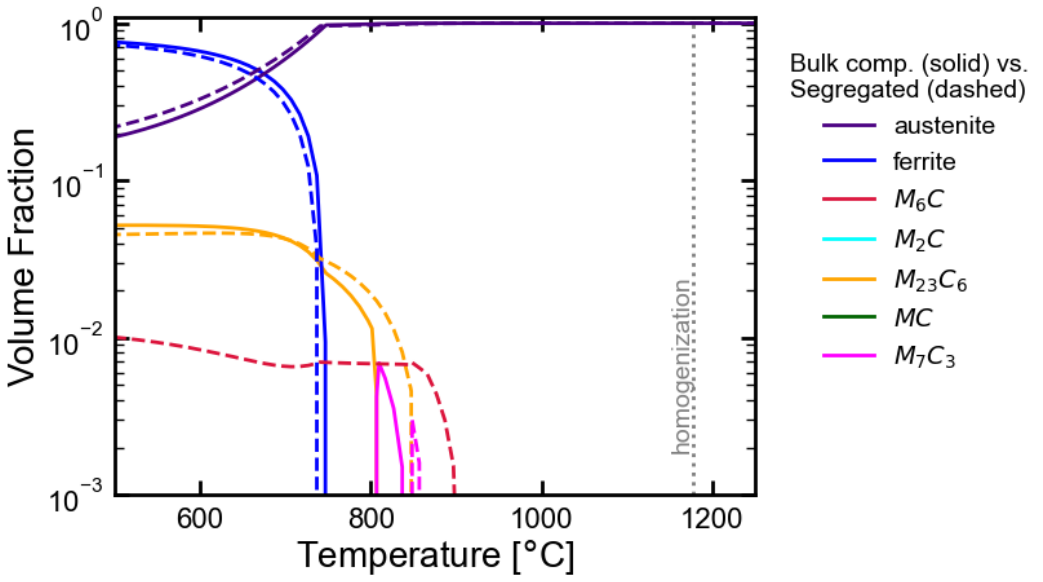

Figure 5. Equilibrium phases for the global composition of AerMet100 (solid lines) compared with the segregated composition (dashed lines). Homogenization was performed at 1177 °C as indicated by the dotted gray line.

The compositions of the M_6C and $M_{23}C_6$ carbides for the bulk and segregated compositions are shown in Figure 6. The M_6C phase is dominated by Mo while the $M_{23}C_6$ is mostly Cr. The difference in the $M_{23}C_6$ phase between segregated and bulk regions is not large, despite the elevated Cr content. However, the elevated Mo content in the segregated region clearly drives a large change in the M_6C behavior. We therefore consider the percent liquid solidification that aligns with the measured Mo segregation ratios found in the literature (Figure 2), not just the AerMet100 alloy discussed here. The median percent liquid that aligns with the observed segregation ratio is 19.4% (see the Appendix, Figure A-3). Therefore, we use the composition at 20% liquid as the segregated region for the remainder of this report.

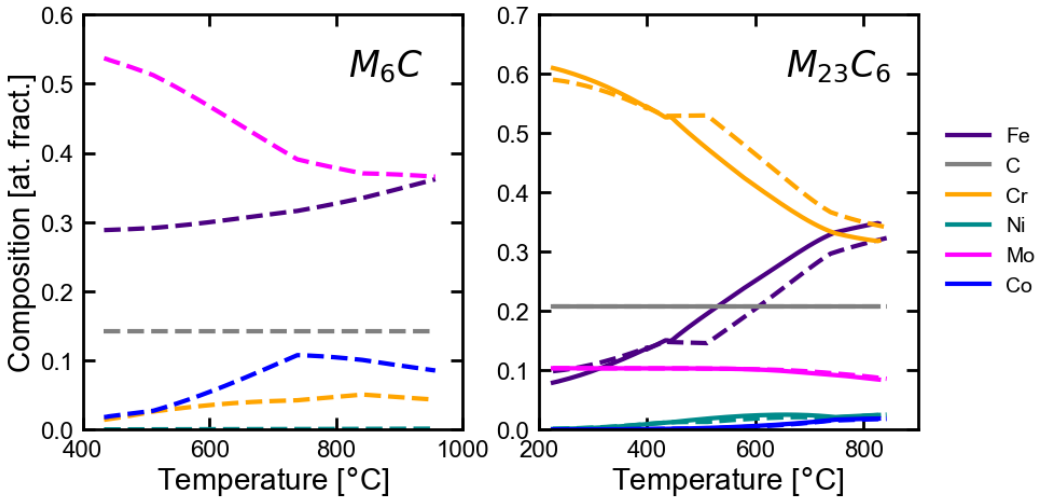

Figure 6. Equilibrium composition of M_6C and $M_{23}C_6$ in AerMet100. Solid lines are bulk composition and dashed lines are segregated composition.

In addition to the difference in the carbides within the segregated regions, a second consideration is the change in the austenite to martensite transformation based on the composition. The start temperature of the martensite transformation (M_S) can be predicted based on composition through various models. Here, we use the Ghosh–Olson model,[23] which incorporates a thermodynamic driving force. The difference between the predicted M_S for the bulk composition and segregated composition is 41 °C. The measured martensitic transformation of AerMet100 is the solid curve in Figure 7; it is an extremely slow transformation that does not fully finish at room temperature. Shifting the curve by the predicted change in M_S between the bulk and segregated regions (ΔM_S), the segregated regions could be expected to only transform up to approximately 90% martensite, meaning there is approximately 10% retained austenite (RA) remaining. Insufficiently stable RA is particularly deleterious to toughness, as it may transform during mechanical loading or during subsequent heat treatments into fresh, brittle martensite. This fresh martensite was observed following tempering in the segregation bands in the Gen3 alloy (Figure 3), which was quenched to room temperature. However, as AerMet100 employs a cryogenic quench to below room temperature (–73 °C) as standard practice due to the sluggish kinetics of even the bulk composition, RA in segregation bands was not directly observed. The processing conditions to mitigate segregation induced microstructural changes (e.g., here with a reduced temperature quench, or above with higher temperature austenitization temperature) can only be designed with some idea of the anticipated behavior.

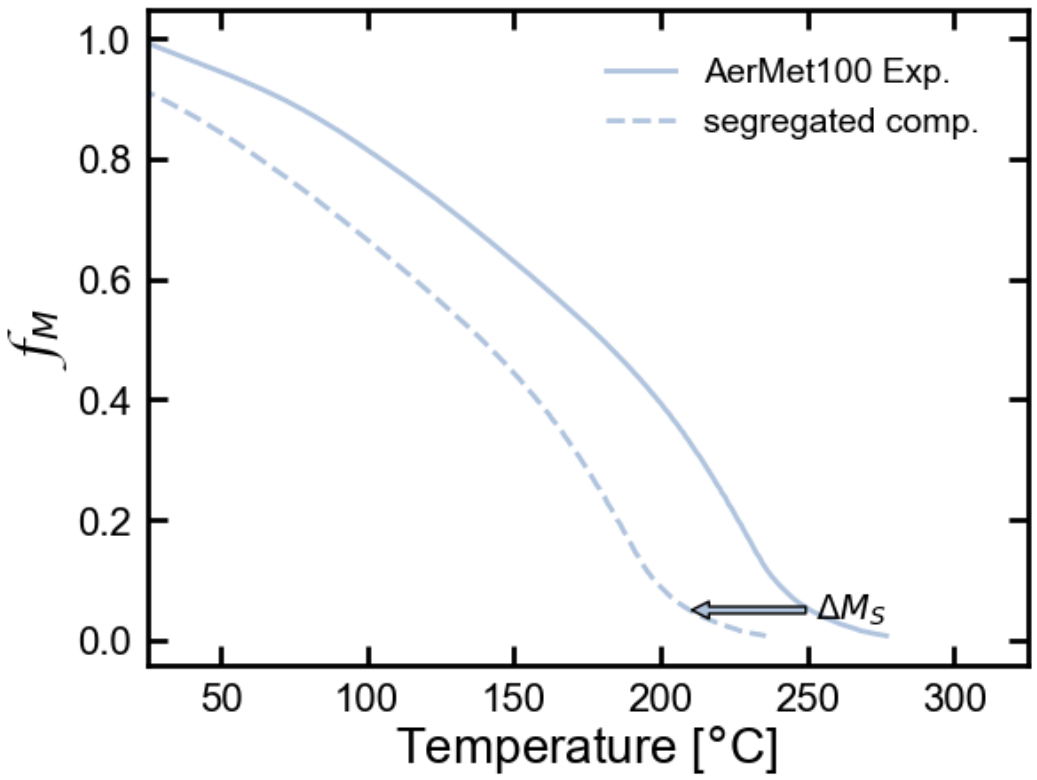

Figure 7. Experimental martensite transformation curve for AerMet100 for the bulk composition (solid line). The curve is shifted by the predicted drop of 41° for the segregated (20% liquid) composition (dashed line).

4. Results

Evaluating the Ni-Co alloys in development, it is most illustrative to start with the Gen3 alloy as it showed the most distinct segregation bands with large carbides, presumed to be M_6C, islands of retained austenite, and fresh martensite. The expected phases present in the bulk versus segregated regions are shown in Figure 8 for the Gen3 alloy with the compositions in Table 4. For the modeled segregated regions, the fraction of the M_6C phase is considerably larger and the solvus extends to much higher temperature, meaning that a higher austenitization treatment would be necessary to dissolve the carbide phase. At an austenitization temperature of 1050 °C, the M_6C should be completely dissolved, whereas in the segregated region there would still be 2.6% remaining. From this it is understood that during austenitization the segregated region was not 100% austenite but a mixture of austenite and M_6C, with the volume fraction of M_6C being unaltered after quenching or tempering. This is consistent with the SEM observations shown in Figure 3 where the segregation bands show a high density of large hexagonal carbides (M_6C).

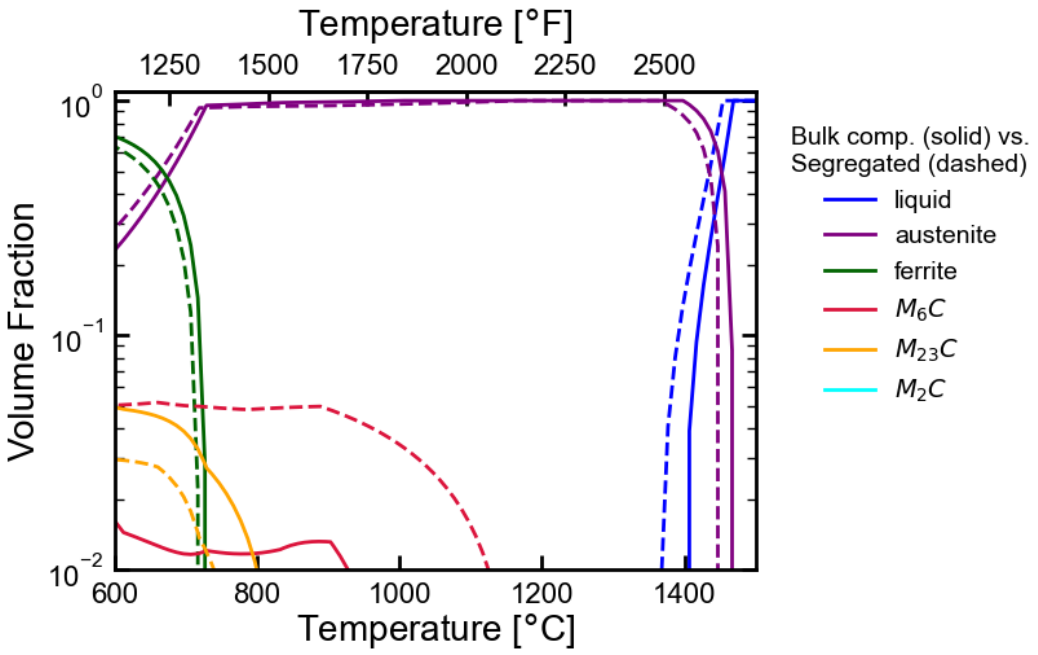

Figure 8. Equilibrium phases for bulk (solid lines) vs. segregated (dashed lines) compositions for Gen3.

Table 4. Comparison of bulk and segregated composition for Gen3 at 20% liquid.

Element	Bulk (wt%)	Segregated (wt%)	Ratio
C	0.28	0.28	1.0
Cr	3.01	3.47	1.15
Mo	1.98	4.07	2.05
Ni	7.68	8.10	1.05
Co	4.89	4.89	1.00
W	1.02	1.74	1.7
V	0.11	0.22	2.02
Mn	0.3	0.43	1.42
Si	0.05	0.05	0.94

4.1 Influence on M_6C

A comparison of the calculated M_6C phase in the segregated composition regions of all the alloys of interest is shown in Figure 9, and the volume fraction at a given austenitization temperature is tabulated in Table 5. Several alloys would still be expected to have an appreciable amount of M_6C remaining after an austenitization treatment. The segregation effect is particularly stark in the Gen3 alloy where M_6C is predicted to be stable even above 1150 °C in the segregated regions.

The addition of W clearly influences the formation of the M_6C phase, particularly when considering the differences in behavior among Gen1 W, Gen1 CrMo, and Gen1 CrMoW and Gen2 compared with Gen2 + W. Figure 10 compares the structure and segregation banding where Gen1 W has the least segregation banding, Gen1 CrMo has some minor banding along the rolling direction (north–south) and the Gen1 CrMoW has some evident segregation. Gen2, Gen2 + W, and Gen3 all have visible segregation banding with Gen3 being the widest and darkest. Also, as a note, Gen3 with its greatest concentration of Mo and W is the only alloy that has M_6C appear in the Scheil solidification path itself, further illustrating the effect of Mo and W to segregate and stabilize the M_6C.This is consistent with what is shown in Figure 9 where the volume fraction (V_F) of M_6C is increasing from Gen1 W to Gen1, CrMo to Gen1 CrMoW, and from the Gen2 alloy to the Gen3 alloy.

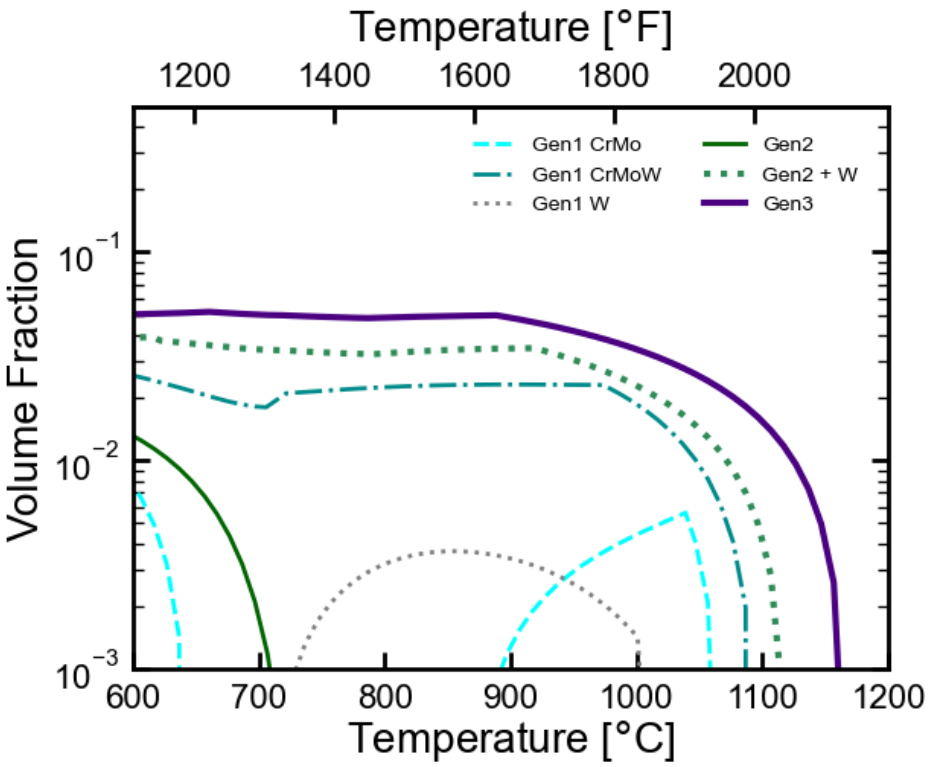

Figure 9. Comparison of the M_6C phase in the segregated region (20% liquid) for various alloys of interest.

Table 5. Volume fraction of the M_6C phase in the segregated region (20% liquid) for alloys of interest.

Alloy	M_6C V_F at 1050 °C	Cr	Mo	W
AerMet100	0	3.0	1.19	0
Gen1 W	0	1.15	1.09	0.47
Gen1 CrMo	0.4	1.76	1.74	0
Gen1 CrMoW	1	1.76	1.74	0.47
Gen2	0	2.75	1.48	0
Gen2 + W	1.5	2.75	1.4	1.07
Gen3	2.6	3.01	1.9	1.02

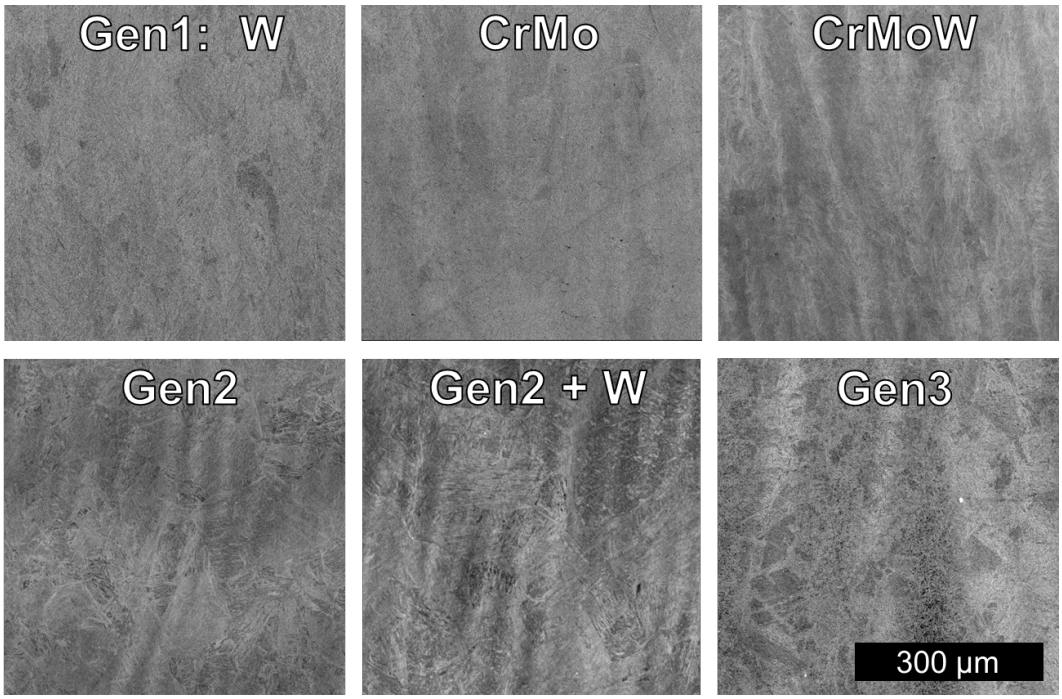

Figure 10. SEM images of segregation bands (or lack thereof) in the alloys.

Regarding the influence of W on M_6C, the composition of the M_6C phase in the segregated region of the Gen3 alloy is shown in Figure 11. In contrast to the AerMet100 alloy (Figure 6), there are stable M_6C phases in both the bulk and segregated compositions and they both have less Mo than the AerMet100 M_6C phase, as the W substitutes on the Mo sites (in sublattice 2).[24] The M_6C phase is also competing with the stable M_2C phase in Gen3 for both the Mo and the W, whereas the M_2C phase is only metastable in AerMet100.

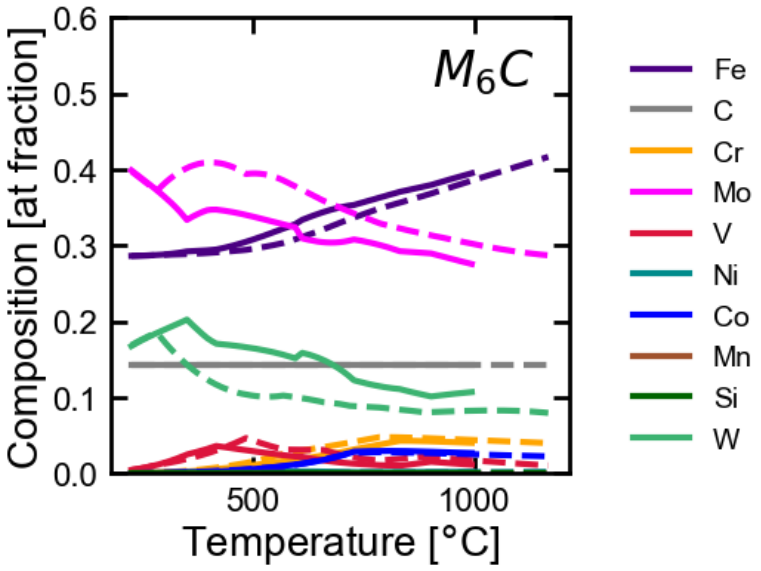

Figure 11. Composition of M_6C for Gen3 in the segregated region (dashed lines) compared with global composition (solid lines).

The Gen3 alloy had an increase in alloying content across the board compared with Gen2 in order to investigate the extent to which M_2C formation could be pushed to obtain higher strengths without lowering the M_S so far as to require cryogenic treatments. It is unsurprising relative to the calculations provided and the observed inhomogeneity in the microstructures that the Mo content was increased too far regarding segregation; however, these extrema provided some benefit toward understanding the mechanical performance of the highly alloyed steel.

To design the next-generation alloy and avoid excessive M_6C formation in segregated regions, we first considered the variation of the controlling elements, Mo and W. From Figure 8 we identify two important pieces of information from the segregated composition: 1) the volume fraction of M_6C that would be present at a given austenitization temperature and 2) the austenitization temperature that would be required to completely dissolve this carbide (i.e., the solvus temperature). The W content was ranged from 0 wt% to 1 wt% and the Mo content was varied from 1 wt% to 4 wt% with the remainder of the composition held constant to the Gen 3 alloy (Table 1). The results are shown in Figure 12.

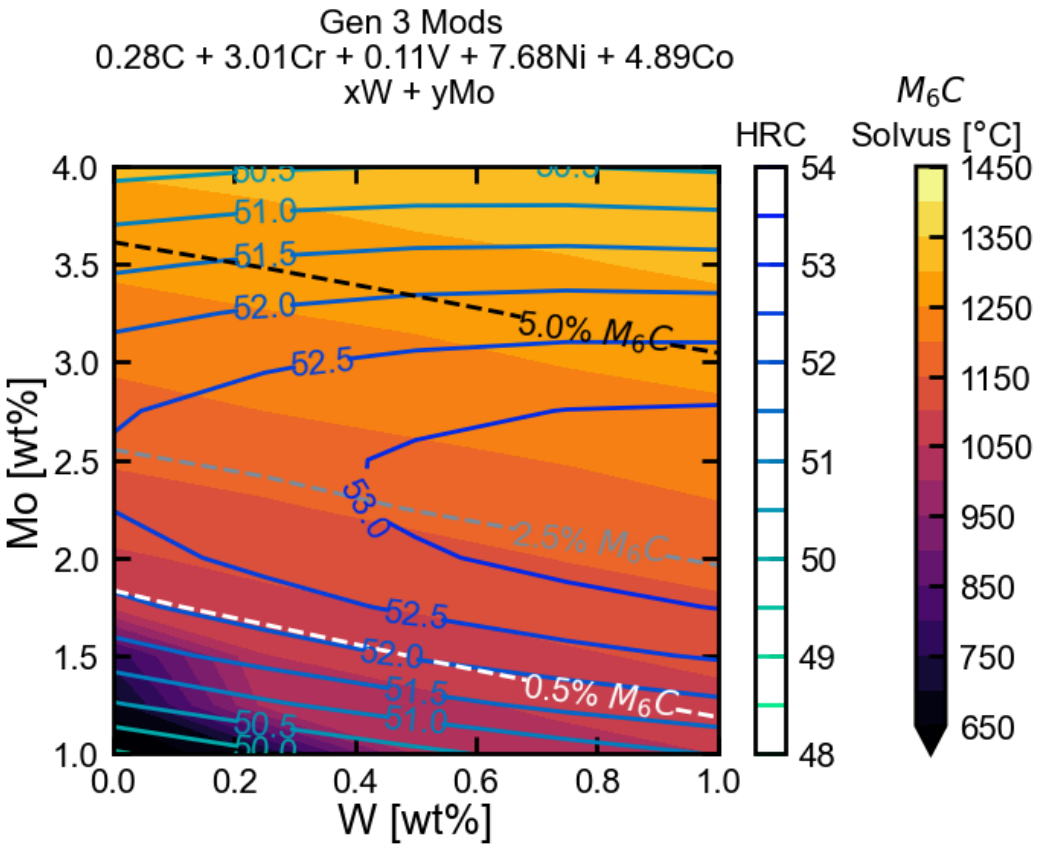

Figure 12. Contour map of M_6C solvus and hardness for variations in W and Mo with the remainder of the elements set at the Gen 3 composition. Dashed contours are predicted V_F of M_6C at 1050 °C.

The volume fraction of M_6C at an austenitization temperature of 1050 °C is indicated by grayscale dashed lines and the solvus temperature of the M_6C is indicated by the colored contours. The hardness of the alloy is predicted using an ML model trained on martensitic steels[25] and is shown by the solid lines in shades of green to blue for increasing Rockwell Hardness C (HRC). An increase in either W or Mo will increase the V_F of M_6C at the austenitization temperature. There is a region of approximately less than 1.5 wt% Mo and less than 0.5 wt% W where the solvus temperature of the M_6C in the segregated material is less than 1050 °C. However, the hardness is expected to decrease as the Mo and W decrease due to the decrease in Mo available to form the M_2C strengthening phase.

While the Cr content likely does not directly influence the M_6C phase, as it is a very minimal component (Figure 11), it may influence the competition between the M_6C and M_2C phase. Therefore, we also consider the variation of Cr with respect to Mo content while keeping the rest of the composition set at Gen3. The results are shown in Figure 13. When varying Cr and Mo, the M_6C V_F and solvus are strongly dependent on the Mo content.

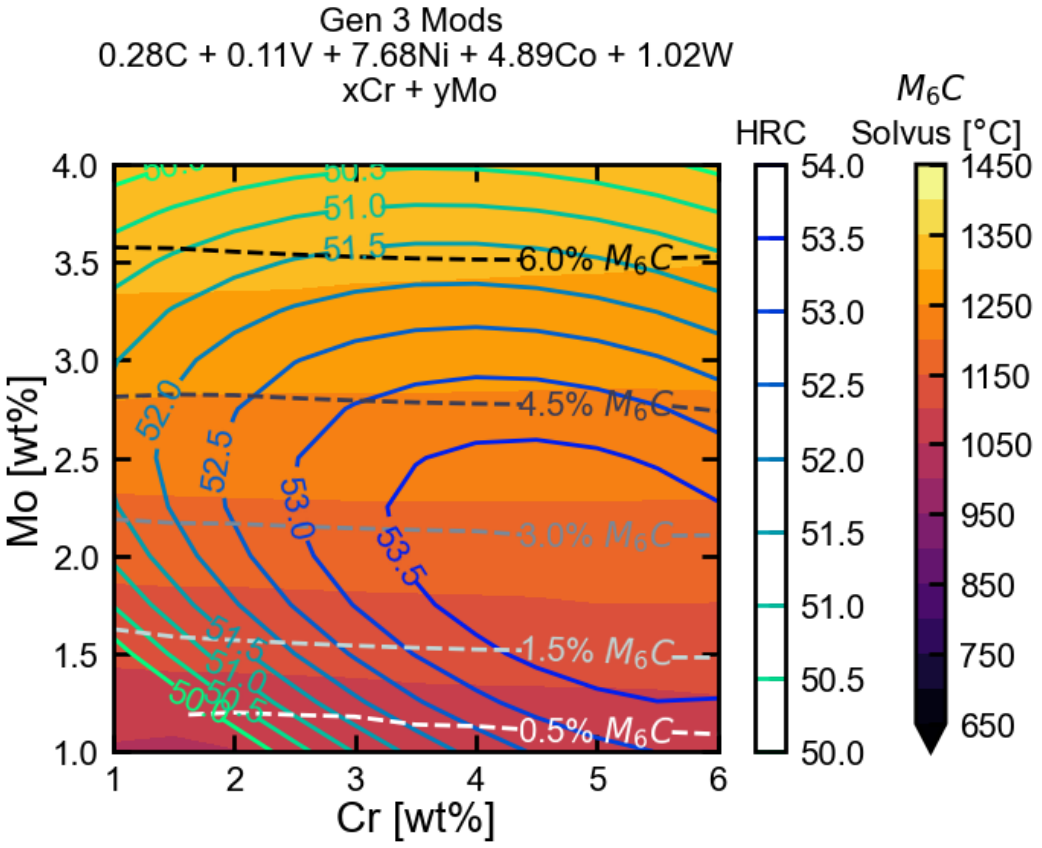

Figure 13. Contour map of M_6C solvus and V_F, and hardness for variations in Cr and Mo with the remainder of the elements set at the Gen 3 composition. Dashed contours are predicted V_F of M_6C at 1050 °C.

Figure 14 shows the difference in varying Cr content at two different levels of W, the original 1.02 wt%, and a lower value of 0.5 wt%, which will reduce the M_6C. Cr having a weak effect on the M_6C formation provides a viable lever to exploit for maintaining strength and not promoting the problematic segregation concerns, M_6C stabilization. We also explored variations in Co and Ni (not shown), as they have negligible effects on the M_6C formation within the segregation portions of the microstructure; this is because they do not segregate heavily, leading to small compositional changes. However, they will be expected to affect the martensite kinetics as discussed below.

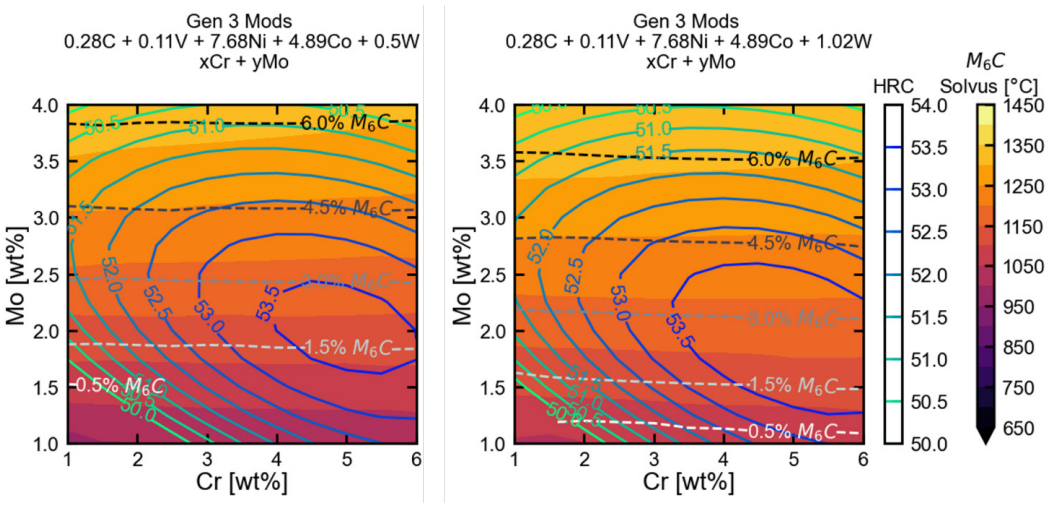

Figure 14. Contour map of M_6C solvus and V_F, and hardness for variations in Cr and Mo with two different levels of W content: (left) 0.5 W and (right) 1.02 W. Dashed contours are predicted V_F of M_6C at 1050 °C.

4.2 Influence on Retained Austenite/Martensite

As noted previously, the enrichment of alloying elements can alter the start (M_S) and kinetics of martensite formation as observed in the AerMet100 case study. In Figure 7, the M_S is shifted because of enrichment in the various elements at the austenitizing temperature. In this case, it is predominantly enrichment of Cr and Ni in the austenite due to much of the Mo and W enrichment being bound up in the M_6C carbides; however, the austenite composition in the segregated region still has higher Mo content than the bulk composition.

To understand the effect of alloy design on the martensite behavior we calculate the change in the M_S temperature between the segregated and bulk composition (ΔM_S). Figure 15 shows the calculated M_S of the bulk austenite composition with the background colored contours and the ΔM_S with the segregated austenite composition in green-scale line contours. The M_6C volume fraction is also plotted as dashed line contours to demonstrate the clear interaction among the microstructural features.

It is interesting to observe that for the low W and Mo concentrations, where M_6C is not stable at the original austenitization temperature, the ΔM_S is as high as 40 °C. As the M_6C becomes more stable and the V_F increases the ΔM_S decreases. This phenomenon is understood to be a function of C, Mo, and W being tied up as the M_6C, and not being available to depress the M_S temperature. These results seem to imply that with proper microstructural design and engineering one can tailor the segregation and M_6C formation to one's benefit.

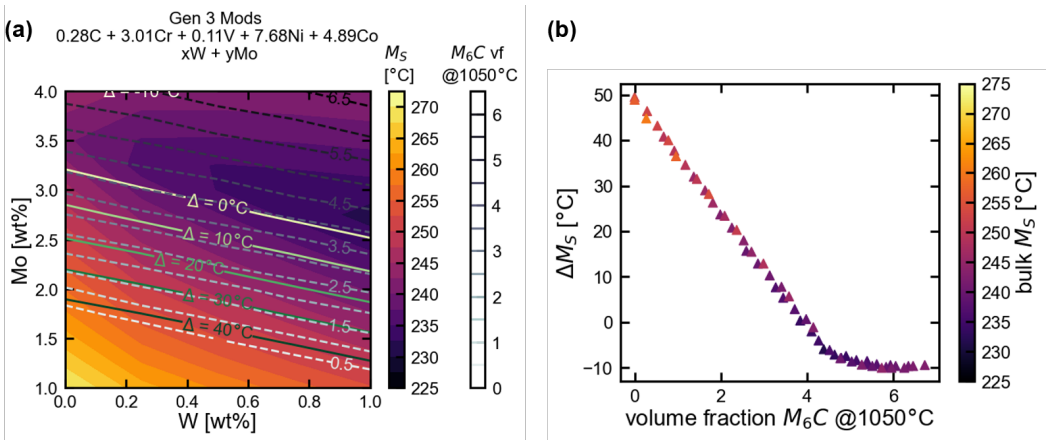

Figure 15. Change in martensite start as a function of (a) alloy and (b) V_F of M_6C.

5. Conclusion

The Scheil solidification modeling results align qualitatively with observed segregation behavior in Ni-Co steels using a 20% cutoff value. While this method is not as precise as rigorous diffusion-based approaches, it is computationally efficient and has more utility for alloy design. The composition of a segregated region as predicted from Scheil modeling is used to determine potential effects of elemental segregation on both carbide and austenite stability. This modeling approach captured both the increase in M_6C and fresh martensite, which were experimentally observed in segregation bands for the Gen 3 alloy. Mo is the most strongly segregating element, consistent with literature reports, and significantly impacts the formation of M_6C carbides in these alloys. W also segregates and promotes the formation of M_6C, substituting on the Mo sites. While Cr also partitions to the segregated regions, it does not significantly influence the M_6C formation, but instead the M_2C, which is desired for strengthening. The austenite composition can also be enriched in these alloying elements, impacting the austenite → martensite transformation. Modeling of the martensite start temperature for the segregated compositions showed a depression of the M_S with respect to Mo and W content, which would lead to an incomplete transformation. However, the increased formation of M_6C with increasing alloy content is actually predicted to reduce the effect on the M_S temperature, as the enriched elements are drawn to the carbide instead of remaining in austenite, offering a possible tool to balance the competing segregation issues.

6. References

1. Pickering EJ, Bhadeshia HKDH. Macrosegregation and microstructural evolution in a pressure-vessel steel. Metall Mater Trans A. 2014;45(7):2983–2997.
2. Slater C, Mandal A, Davis C. The influence of segregation of Mn on the recrystallization behavior of C-Mn steels. Metall Mater Trans B. 2019;50(4):1627–1636.
3. Torkar M, Vodopivec F, Petovar S. Analysis of segregations in as-cast X40CrMoV51 steel. Mater Sci Eng A. 1993;173(1–2):313–316.
4. Lippard H et al. Microsegregation behavior during solidification and homogenization of AerMet100 steel. Metall Mater Trans B. 1998;29(1):205–210.
5. Roy S et al. Prediction of inhomogeneous distribution of microalloy precipitates in continuous-cast high-strength, low-alloy steel slab. Metall Mater Trans A. 2012;43(6):1845–1860.
6. Sakasegawa H, Tanigawa H. Microsegregation in a F82H plate. J Nucl Mater. 2013;442[1, Suppl 1]:S18–S22.
7. Sawada K, Sekido K, Kimura K. Segregation and its effect on creep rupture strength in Grade 92 steels. Mater Charact. 2020;169:110581.
8. Krugla M et al. Microsegregation influence on austenite formation from ferrite and cementite in Fe–C–Mn–Si and Fe–C–Si steels. Metals. 2024;14(1):92.
9. Poirier D, Flemings M. Investigation of solidification of high-strength steel castings. Army Materials Research Agency (US); 1965. Accession No.: AD0645346.
10. Yan G et al. Effect of macrosegregation on the microstructure and mechanical properties of a pressure-vessel steel. Metall Materi Trans A. 2017;48(7):3470–3481.
11. Torkar M, Vodopivec F, Petovar S. Analysis of segregations in as-cast X40CrMoV51 steel. Mater Sci Eng A. 1993;173(1):313–316.
12. Jabar S et al. The effect of micro-segregation on the quantification of microstructural parameters in grade 91 steel. Metall Mater Trans A. 2021;52:426–437.

13. Bregeault M et al. Evolution of carbon distribution across meso-scale segregations in pressure vessel steel. Mater Today Commun. 2025;44:112024.

14. Bee C et al. Micro-segregation induced strain inhomogeneity in >900 MPa UTS martensitic hot rolled advanced high strength steel. Mater Sci Eng A. 2023;888:145335.

15. Davis C, Strangwood M. Segregation behaviour in Nb microalloyed steels. Mater Sci Technol. 2009;25(9):1126–1133.

16. Webb T, Van Aken D, Lekakh S. Evaluating chemical homogeneity in the performance of Eglin steel. AFS Trans. 2014;122:317–333.

17. United States Steel Corporation. The making, shaping and treating of steel. 8th ed. United States Steel; 1964.

18. Andersson JO et al. Thermo-Calc & DICTRA, computational tools for materials science. Calphad. 2002;26(2):273–312.

19. Athavale VA. Development of stage-I tempered high strength cast steel for ground engaging tools. Missouri University of Science and Technology (US); 2019.

20. Field D et al. Heat treatment design to modify the martensite misorientation and obtain superior strength–toughness combinations. Metall Mater Trans A. 2020;51(3):1038–1043.

21. Field DM et al. Heat treatment and austenitization temperature effect on microstructure and impact toughness of an ultra-high strength steel. Metals. 2021;11(5):723.

22. Athavale V et al. Mechanical properties and impact wear resistance of 540 Brinell hardness Mn-Si-Mo-V steel. 123rd AFS Metalcasting Congress; 2019; Atlanta, GA.

23. Ghosh G, Olson G. Kinetics of FCC→ BCC heterogeneous martensitic nucleation—I. The critical driving force for athermal nucleation. Acta Metall Mater. 1994;42(10):3361–3370.

24. Frisk K, Bratberg J, Markström A. Thermodynamic modelling of the M6C carbide in cemented carbides and high-speed steel. Calphad. 2005;29(2):91–96.

25. Murdoch HA et al. Tempered hardness optimization of martensitic alloy steels. Integr Mater Manuf Innov. 2023;12(4):301–320.

Appendix. Parameter Studies

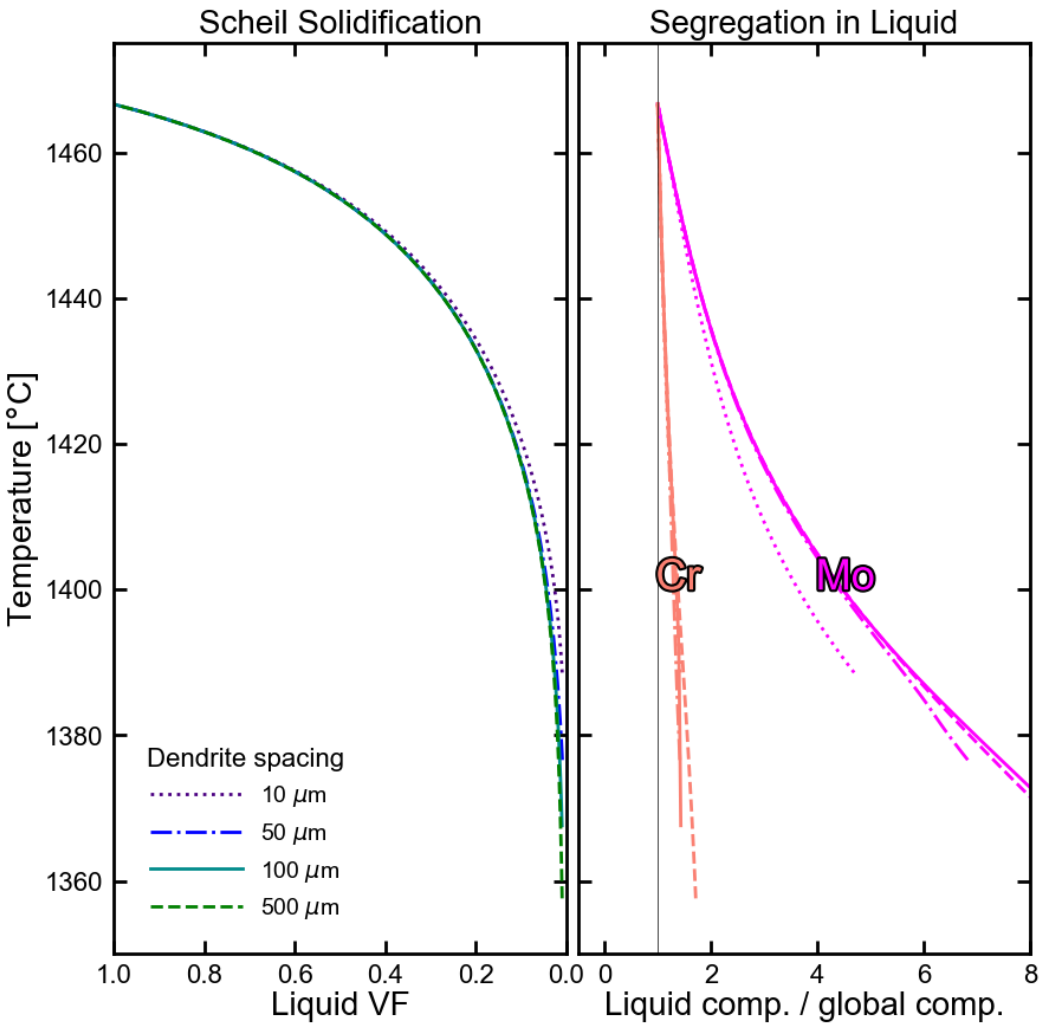

Figure A-1. Parameter study of dendrite spacing for Scheil calculation with back diffusion using AerMet100.

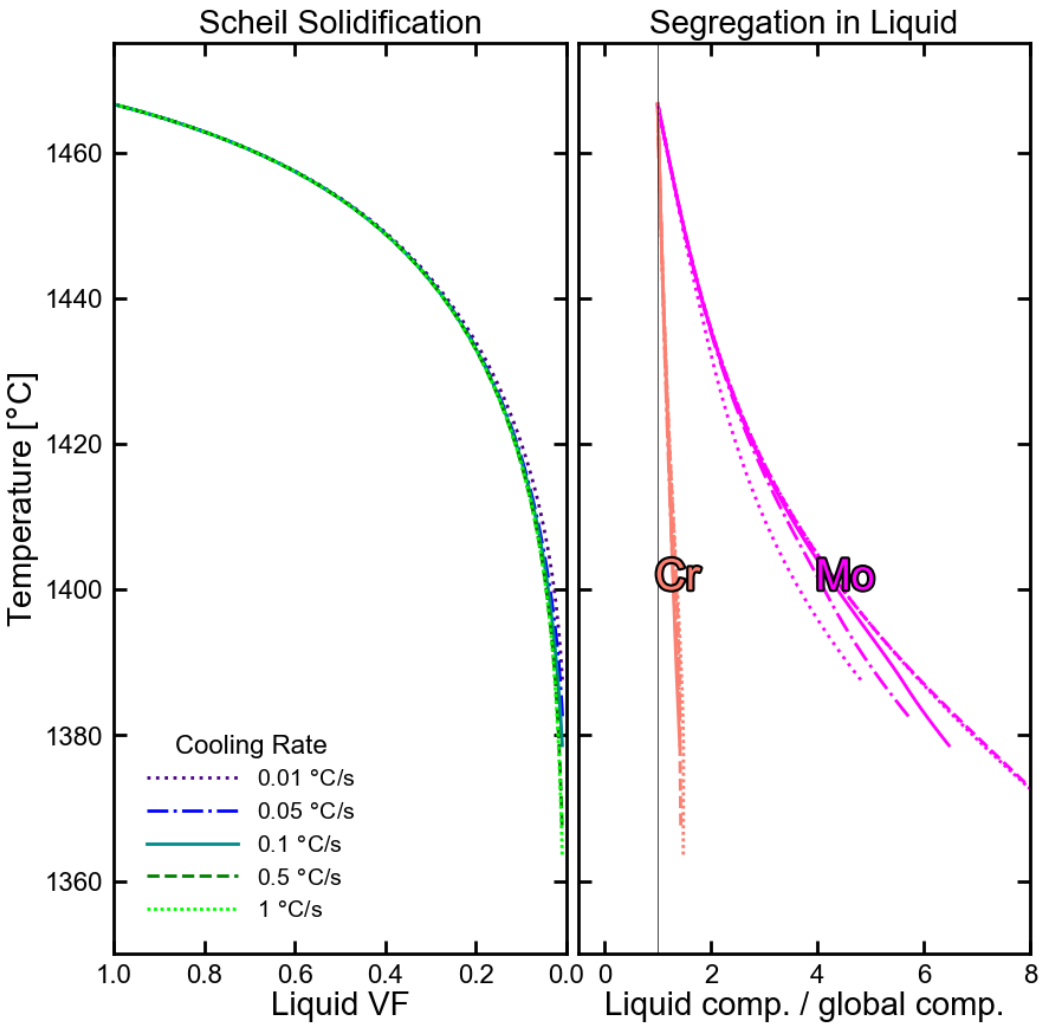

Figure A-2. Parameter study of cooling rate for Scheil calculation with back diffusion using AerMet100.

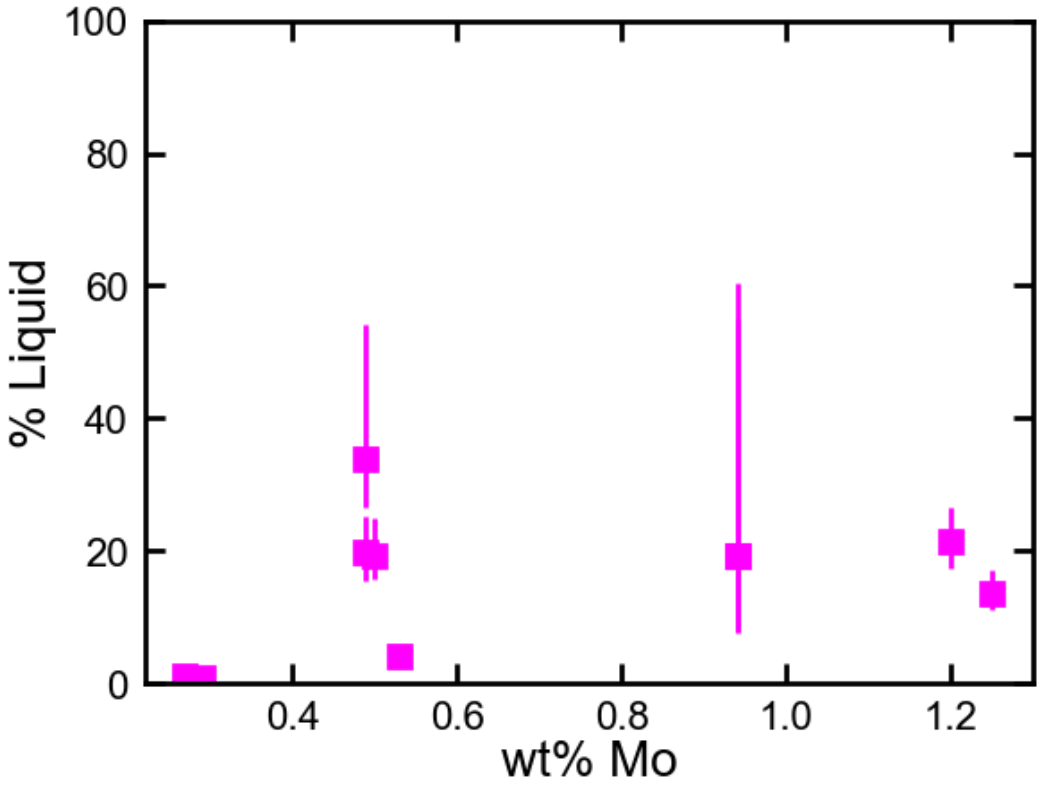

Figure A-3. Percent liquid during solidification that corresponds to the reported experimental segregation ratio for molybdenum (Mo) error bars are ±10% on the exp. ratio.

List of Symbols, Abbreviations, and Acronyms

C	Carbon
Co	Cobalt
Cr	Chromium
DICTRA	Diffusion Controlled Transformations
Fe	Iron
fM	Fraction of Martensite
Gen	Generation
HRC	Rockwell Hardness C
ML	Machine Learning
Mn	Manganese
Mo	Molybdenum
M_S	Martensite Start Temperature
Ni	Nickel
RA	Retained Austenite
SEM	Scanning Electron Microscope
Si	Silicon
UHSS	Ultra-High-Strength Steels
V	Vanadium
VAR	Vacuum Arc Remelting
V_F	Volume Fraction
W	Tungsten
wt%	Weight Percent

1 (PDF)	DEFENSE TECHNICAL INFORMATION CTR DTIC OCA
1 (PDF)	DEVCOM ARL FCDD RLB CB TECH LIB